Solutions for Homework #3

Problem 1 – Numerical phantom

For starters, let us look at the original numerical phantom image. It has only a real component, there is no phase or imaginary component.

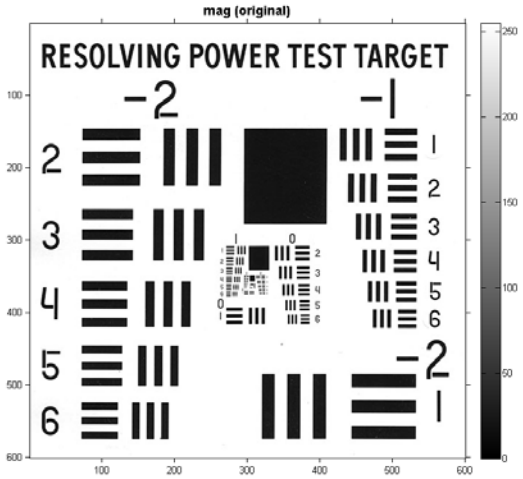

Fig 1.1: The original numerical phantom

a) The k-space data are readily generated via a 2D Fourier transform. The data have 600 sample points in x and y as well as in kx and ky. The center of k-space is located in the centers of those images. Note the symmetry because the image data are real-valued only.

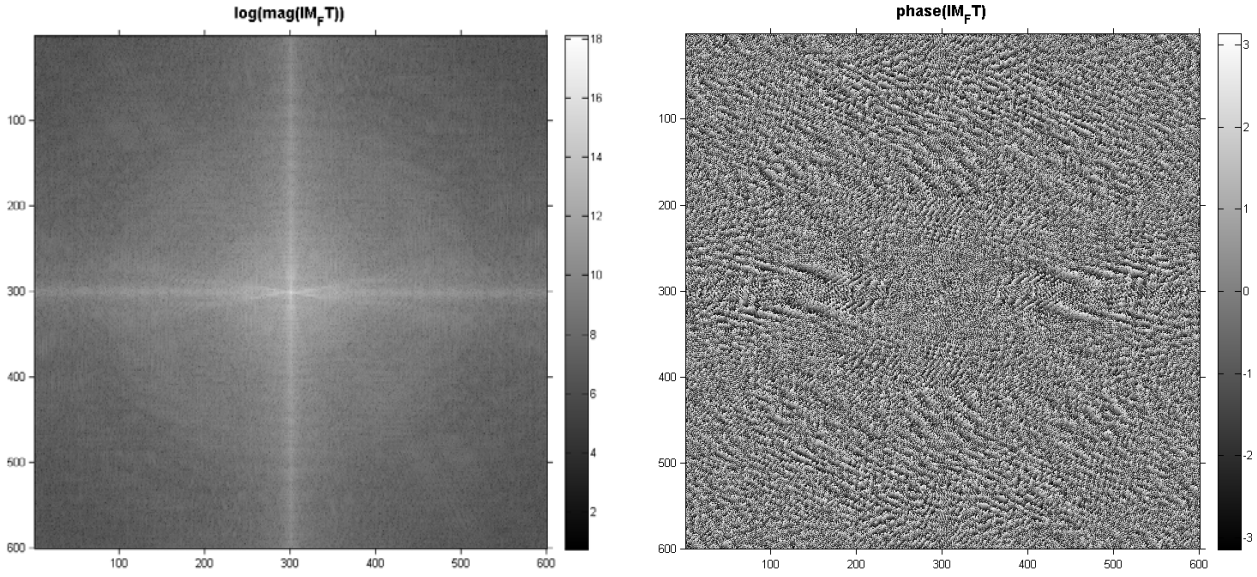

Fig 1.2 K-space data of the numerical phantom shown as magnitude on logarithmic scale (left) and phase in radians (right)

b) Let's start with the new k-space representation. The outer 50 percent of rows are discarded (25% on top, 25% on the bottom). The new raw data matrix size is reduced to 300 rows.

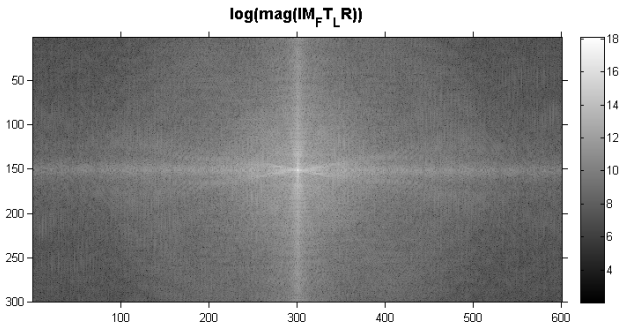

Fig. 1.3: K-space representation with partial Fourier in ky (reduction by 50% to 300 rows). The center of k-space is in the center of the image. According to Matlab notation for a even number of rows and columns, its location is column index 301 and row index 151.

A simple 2D DFT will generate the corresponding images:

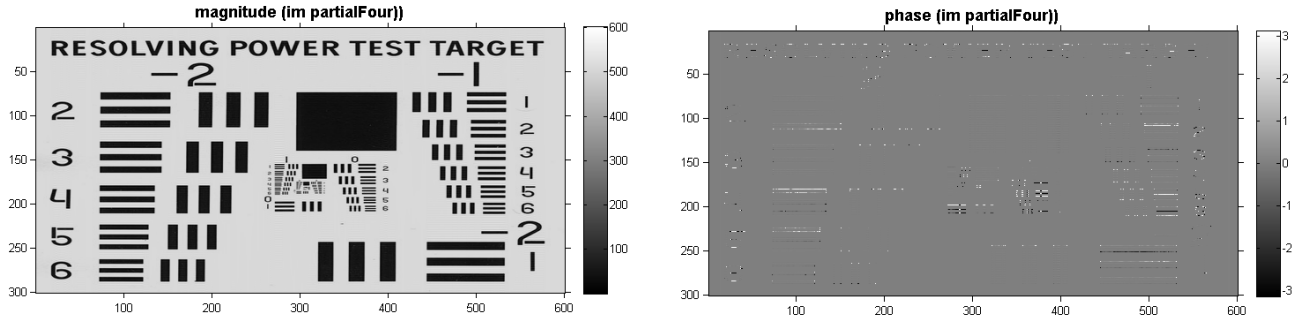

Fig. 1.4: Magnitude and phase of the numerical phantom reconstructed with a 50% partial Fourier reconstruction in ky.

The sampling intervals in k-space remained constant but the highest sampled spatial frequency was reduced by a factor of two. There are twice as many samples in the readout direction as compared to the phase encoding direction. Consequently, the spatial resolution is reduced and now anisotropic. The resolution patterns can be better resolved in the x-direction than in the y-direction. Also, the aspect ratio is improperly displayed without modifications (see c). In theory, the signal-to-noise ratio is increased because the voxels have increased in size.

The imaging time is cut in half because only half as many k-space lines (echoes) are acquired. The gradients in x and z are unaffected by the changes but the maximum gradient strength required for the phase encoding is reduced by a factor of two also.

c)
In the resulting image, the aspect ratio of the voxels should be twice as long in the y-direction as in the x-direction. The image needs to be ‘stretched’ in the y-direction to properly display the geometric aspect ratio. This could be accomplished by spatial interpolation, e.g. a splines. Most commonly though, this is done by zerofilling as discussed in class. Zero-filling is equivalent to a sinc interpolation in image space. It does not improve the ‘acquired spatial resolution’.

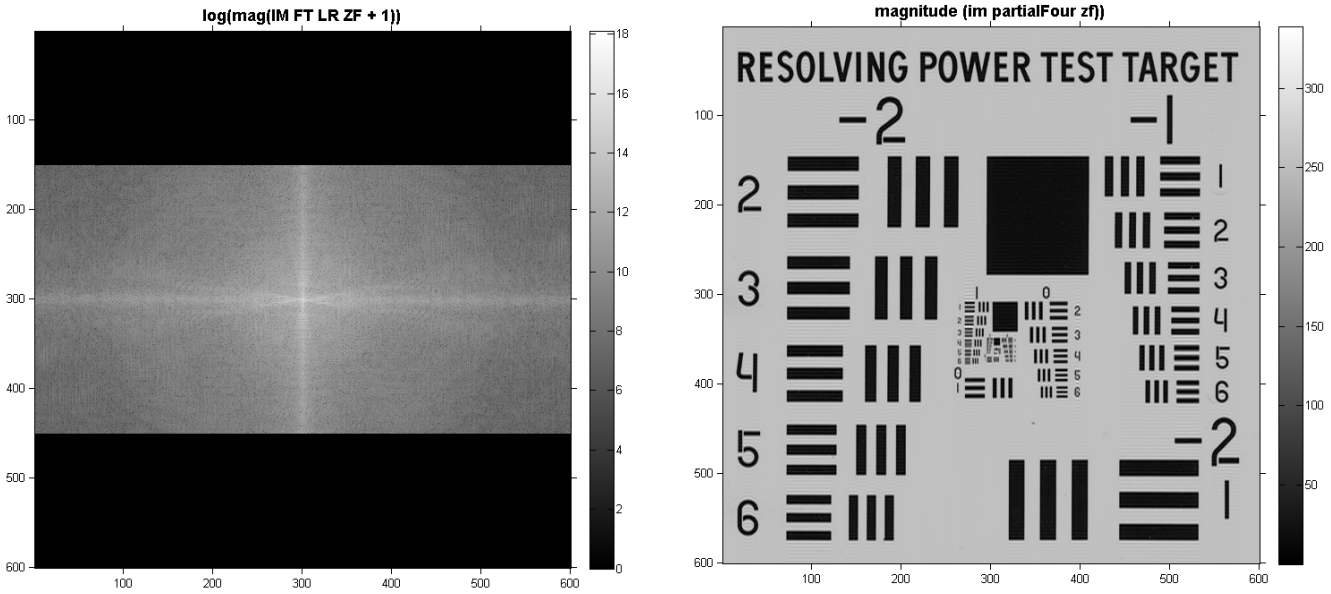

Fig 1.5 Zero-filled reconstruction to fix the aspect ratio of the partial Fourier acquisition. The outer lines of k-space are filled with zeros (left) and the proper aspect ratio is restored (right).

d) The sharp edge in k-space transitioning from spatial frequencies with energy to the zero-filling band (c) or to no data (b) causes a truncation artifact, also called Gibb's ringing in the image domain. This can be compensated by a smoother transition through low-pass filtering, e.g. with a Hanning window.

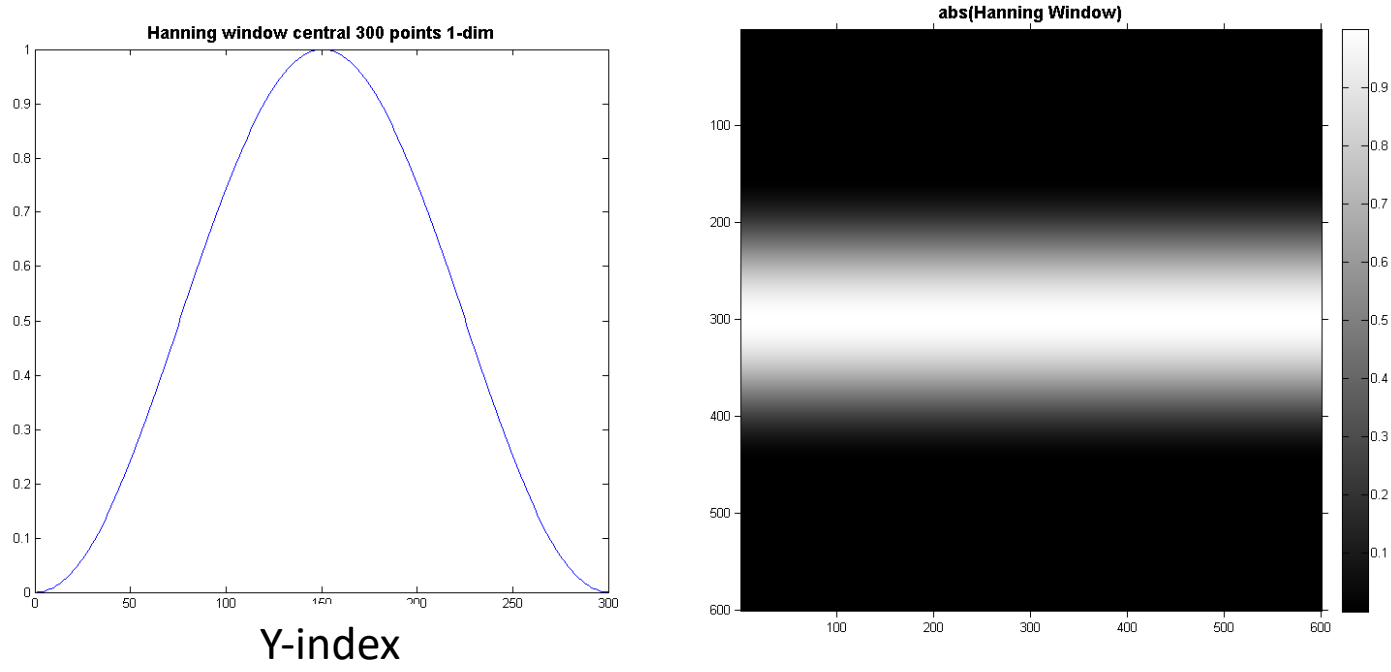

Fig 1.6: A low-pass filter is used to smooth the transition of the k-space edge. In this example, it is accomplished with a Hanning filter shown as a profile on the left and as a k-space matrix of weighting coefficients on the right.

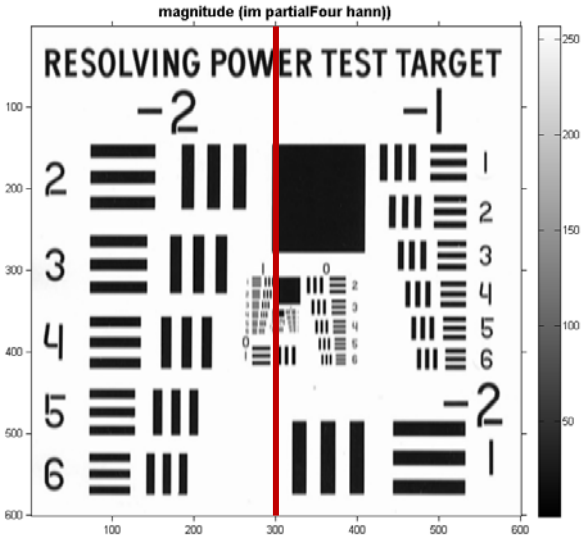

Fig. 1.7: The resulting image reconstructed with partial Fourier acquisition and a low-pass filter. The location of the line profile in Fig. 1.8 is shown on red.

The image reconstructed with this approach has reduced ringing on high contrast edges as shown in the line profiles in Figure 1.8.

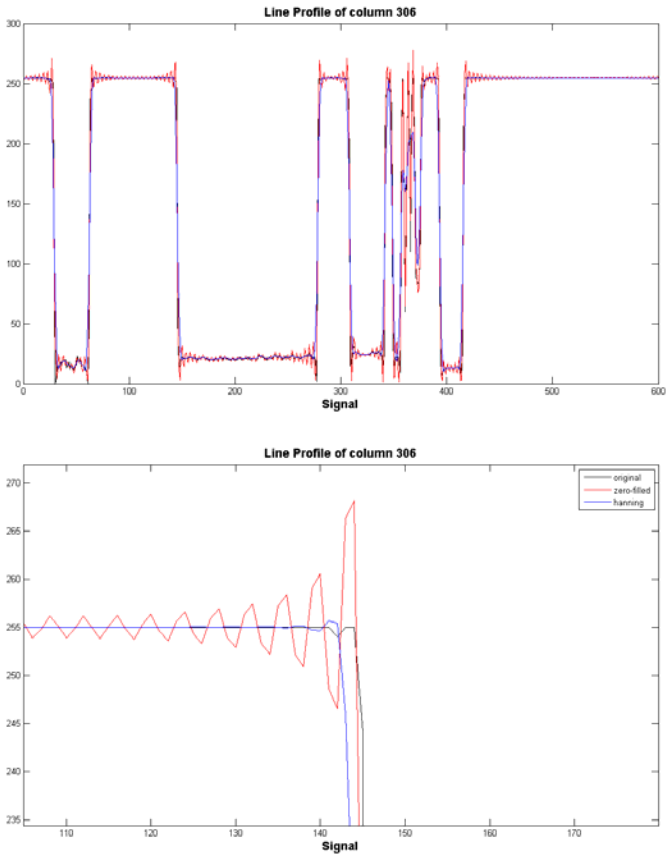

Fig. 1.8: line profile from a position shown in Fig. 1.7. Notice the ringing and smotthing but edge displacement with the low-pass filtered approach as compared to the original high resolution image.

The line profiles and images in zoomed mode also show the drawback of the low-pass filtering: smoothing is introduced that further reduces the acquired spatial resolution.

1e) Now we kept the highest spatial resolution consistent with the full resolution acquisition but we discarded every other ky line. In other words, our Δky has doubled. Consequently, the FOV is reduced in half and the resulting image suffers from spatial aliasing, the so-called fold-over artefact.

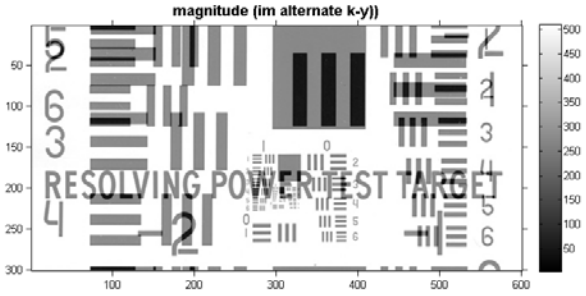

Fig 1.9 Image reconstructed with every other k-space line, suffering from fold-over artefact in the y-direction.

Problem 2 –Phantom acquired in MR scanner

2a) The k-space data as read in by the raw data file.

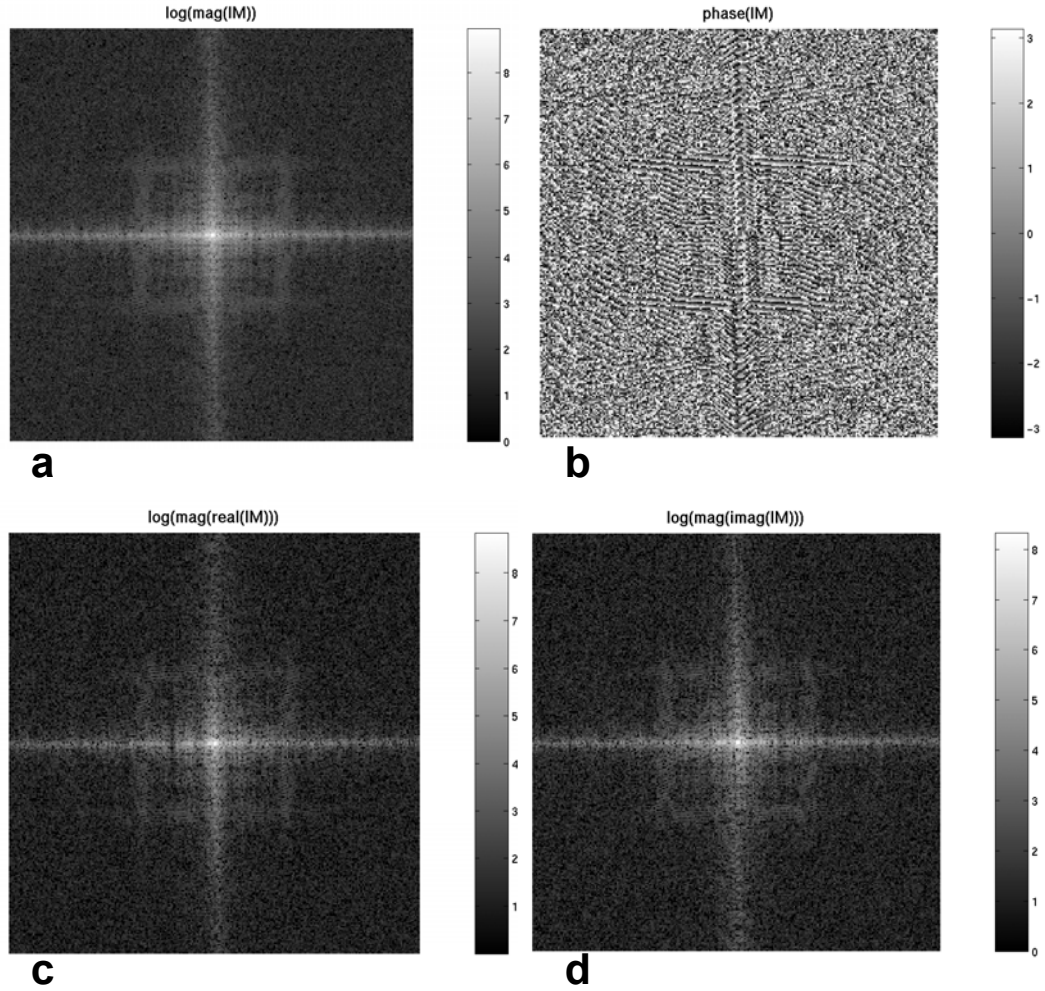

Fig. 2.1 The magnitude (a), phase (b), real (c), and the imaginary (d) component of the acquired k-space data. This scan consisted of 256 samples in the readout direction and 256 phase encodes.

The k-space data have some similar features in that the central spatial frequencies contain most of the energy. However, some of the structured patterns also cause high signal intensities in k-space mimicking the outline of a square in k-space. These bands consist mostly of the spatial frequencies which define the squared small resolution pattern.

The real and the imaginary channel represent the signal acquired with two channels of a quadrature receive coil. Both channels contribute similar energies for the image reconstruction. While the phase distribution in Fourier space seems more or less chaotic, it is very crucial to the image reconstruction.

2b) The reconstruction can be performed with a standard 2D inverse Fourier Transform. The magnitude, phase, real, and imaginary components of the image are shown in Figure 2.2 with a linear grayscale.

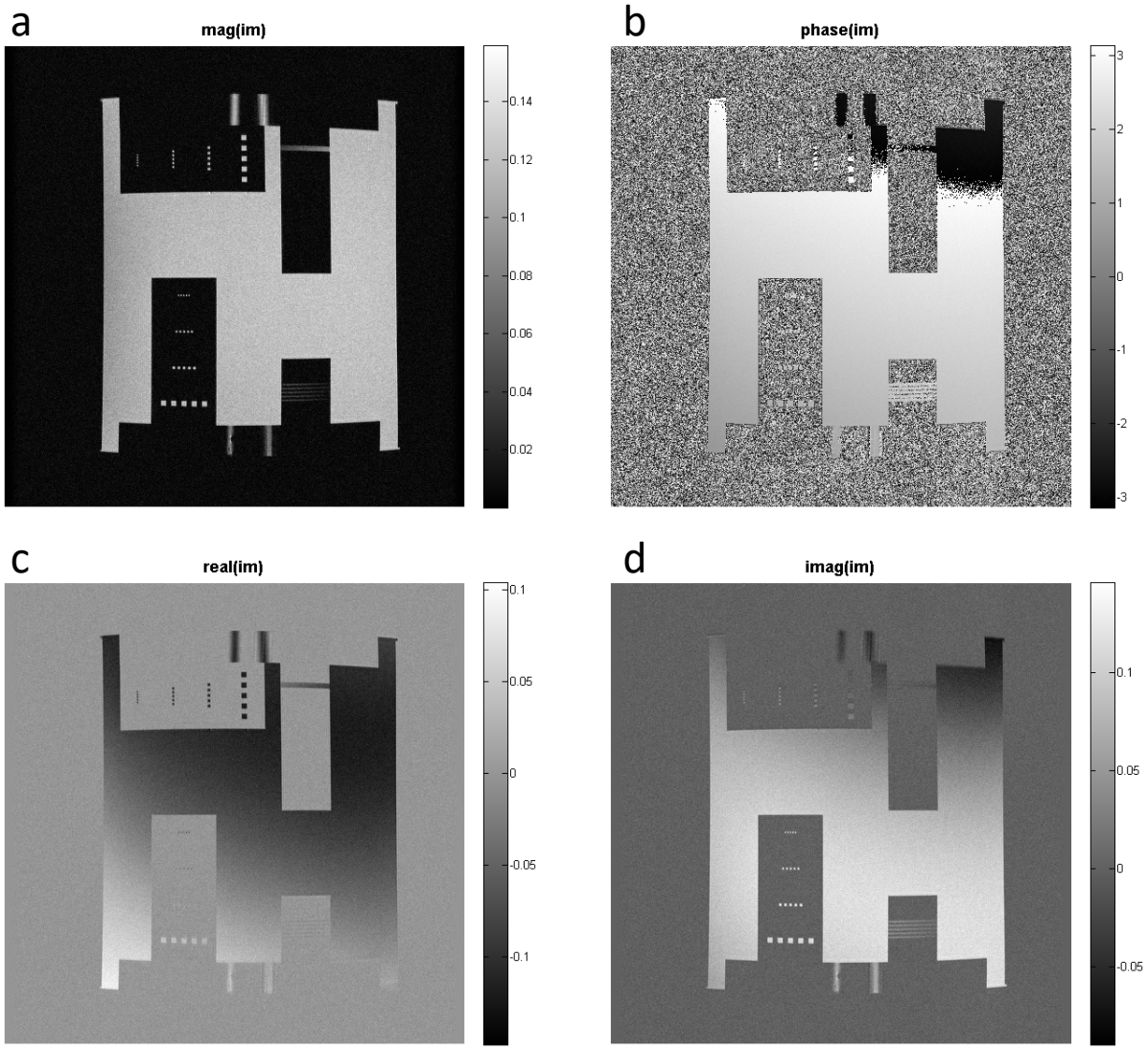

Figure 2.2: *The magnitude (a), phase (b), real (c), and imaginary (d) channel of the image reconstructed from a 256x256 complex matrix.*

In object space, the real and the imaginary channel contain similar signal energies as well. The phase is slowly varying across the object and appears randomly distributed outside the object. Since air does not contain any hydrogen atoms, there is no signal and the reported phase simply describes the phase of the noise. In an ideal MRI system, the image would be perfectly encoded by a homogeneous static magnetic field and a linear gradient system and all spins were on resonance. In this case, only the real channel in object space would contain any energy and the object would have no phase. However, local field inhomogeneities caused by system imperfections and magnetic susceptibilities at boundaries of different tissues introduce phase variations.

2c) This image requires Ny = 512 phase encodes and each phase encode takes TR = 425 ms. The total scan time is Ny*TR = 512*.425 s = 217.6 s
2d) The receiver bandwidth is BW = 20.83 kHz, the duration of the phase encoding τ_y = 1 ms, the slice thickness Δz = 0.2 cm, and the bandwidth of the excitation pulse BW_1 = is 1250 Hz.. Using equations 5.79 from the Nishimura textbook: $\gamma * g_x * \Delta t * FOV_x * = 2*\pi$ and $\gamma * g_{yi} * \tau_y * FOV_y * = 2\pi$:
readout gradient: gx = $BW/(\gamma/(2\pi)*FOV_x)$ = 2.72 *10^(-5) T/cm = .272 G/cm
maximum phase encoding gradient: gy = $256/(\gamma/(2\pi)*\tau_y *FOV_y)$ = 3.34 *10^(-4) T/cm = 3.34 G/cm
slice encoding gradient: gz = $BW\_1/(\gamma/(2\pi)*\Delta z)$ = 1.46*10^(-4) T/cm = 1.46 G/cm

2e) Fig. 2.3 shows the reconstructed magnitude and phase image after mimicking a partial Fourier acquisition with only 256 ky lines and zerofilling for the proper aspect ratio.

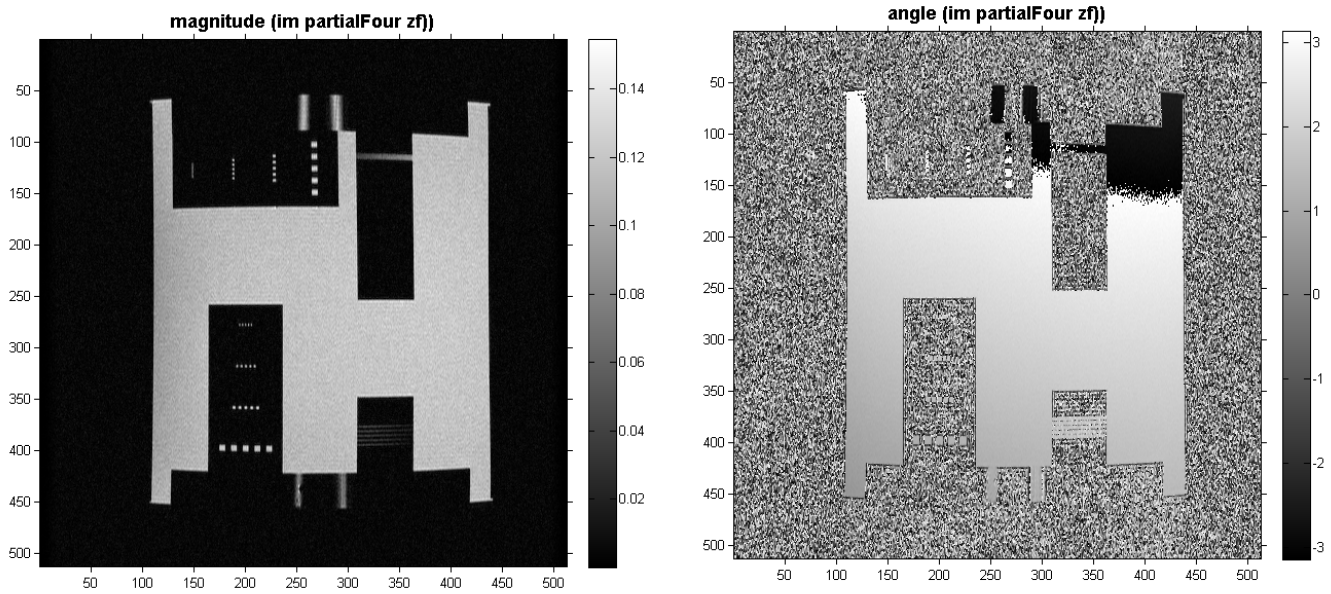

Fig. 2.3: Data reconstructed from a simulated partial Fourier acquisition and with zero-filling in the ky direction.

Compared to the full resolution image, a loss in spatial resolution is noticeable in the phase encoding direction as shown in Fig. 2.4. Also, the SNR has increased because the acquired voxel size is bigger.

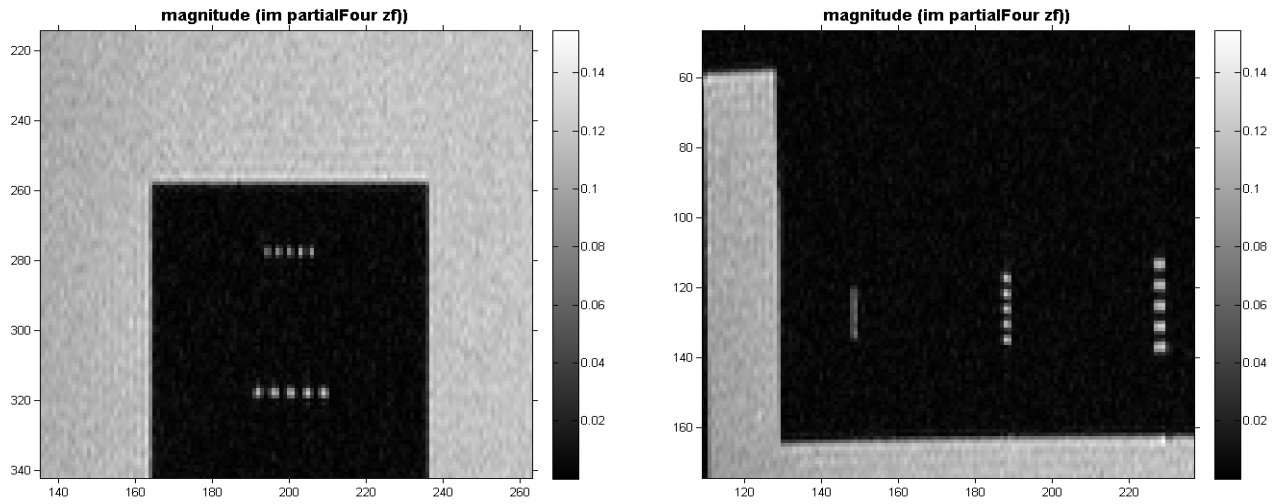

Fig 2.4¨Zoomed in regions of the phantom showing superior resolution in the readout direction (512 samples – left figure) as compared to the phase encoding direction (256 samples – right figure).

2f) Signal to Noise Analysis

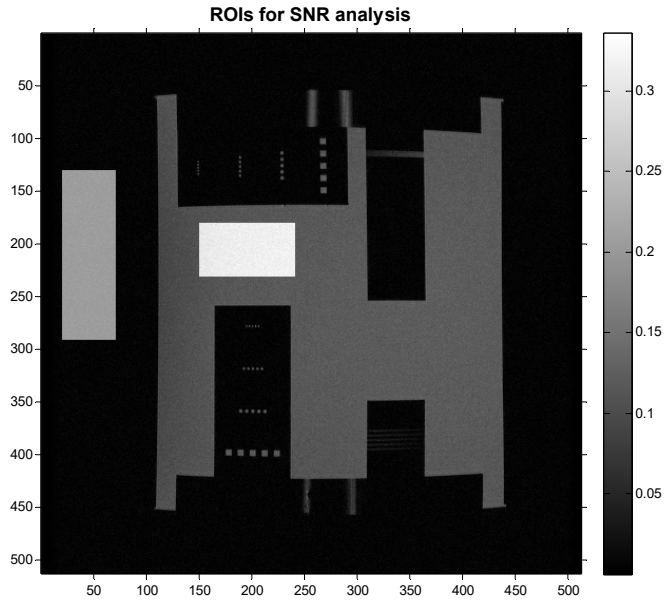

Fig 2.5: The regions of interest for the ROI analysis are shown as superimposed squares on the gryyscale image.

The two region method is a decent approach for the SNR estimation here. As shown in Figure 2.5, two ROIs are drawn: one in air for the noise estimate from the standard deviation and and one in a phantom region with relatively constant signal estimated from the mean. The SNR is then determined as the ratio.

For the fully sampled image, the estimates SNR is 29.6.
For the image reconstructed with partial Fourier imaging, the estimated SNR is 42.1
The fundamental SNR equation in MR states that the SNR is proportional to the voxel size and the square root of the acquisition time. Let us look at the fully sampled 512x512 image as the baseline. In comparison, the partial Fourier reconstructed image has twice the voxel size. Also, the imaging time has

decreased by a factor of 2. Therefore, we expect an SNR gain by a square root of 2 for the partial Fourier acquisition..

The theoretical changes in SNR (factor of 1.41) and the measured changes in SNR (factor of 1.42) line up pretty well. The difference in the SNR of the images is well noticeable by visual inspection. A rule of thumb is that an SNR difference of 10% will have an effect on the image quality that can be noticed by the human eye.

When a multi-receiver coil is used, this simple SNR analysis is not valid anymore. The typical approach for combining signal from multiple; receiver coils is the sum of squares of each individual receiver channel. The introduction of multiple coils would cause spatially varying noise, meaning that the two-region method would no longer be an effective way to evaluate SNR. Acquiring multiple images of the same slice and performing the subtraction SNR method may be a more desirable alternative. Things get even more complicated if accelerated imaging is used (parallel MRI, compressed sensing etc.) but that is beyond the scope of this question.

Problem 3 In vivo data

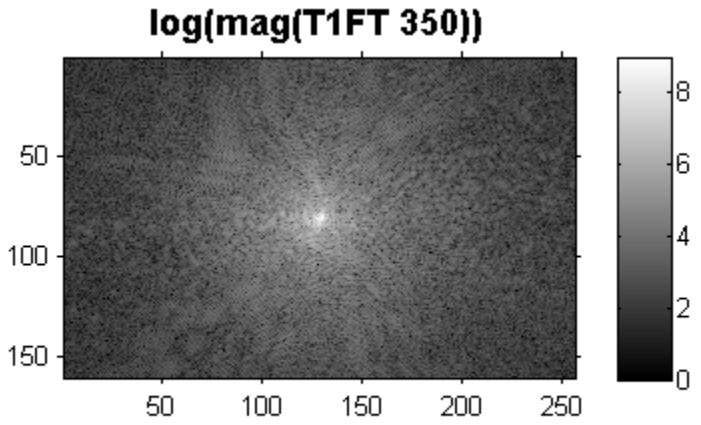

Fig 3.1: Magnitude of k-space data on a logarithmic grayscale.

3a) Fig. 3.1 shows the magnitude representation of k-space on a log scale. Again, the highest energies can be found at the central spatial frequencies. The biological object does not show the structured k-space patterns that were generated by the numerical and the high res phantom seen in problems 1 and 2.

3b) The image has to be zero-padded from 160x256 to a 256x256 image matrix.

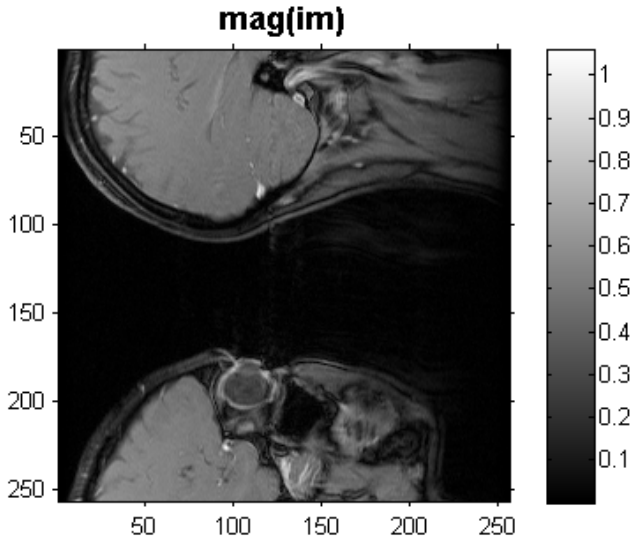

Fig 3.2: T1-weighted image reconstructed with zero-filling.

3c)
Every other column of the raw data is now multiplied with –1. This multiplication of the raw data with $\exp(-i\pi n)$ causes a shift of the object in image space by half a field of view (Fourier shift theorem). The data have been already multiplied in such a way for every other row so that we can skip all fftshift commands after multiplying every other column. In order to provide the proper phase of the object in image space, these multiplications need to be performed in image space also since we did not perform a fftshift prior to the FFT. However, since we are only interested in the magnitude image here, this step can be left out.

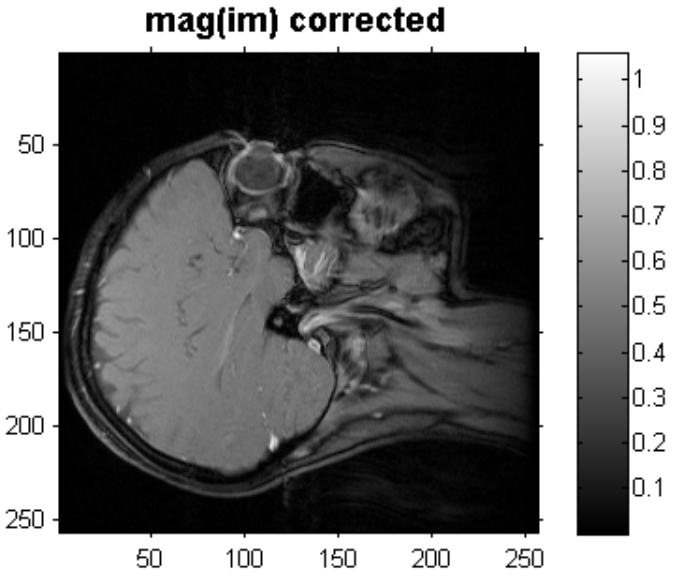

Fig 3.3: Image reconstructed with the proper FOV shift as applied via k-space phase modification.